Cite as: Balzter, H., Baker, J.R., Tomppo, E. and Hallikainen, M. (2002): Retrieval of timber volume and snow water equivalent over a Finnish boreal forest from airborne polarimetric Synthetic Aperture Radar. International Journal of Remote Sensing 23, 3185-3208.

Retrieval of timber volume and snow water equivalent over a Finnish boreal forest from airborne polarimetric Synthetic Aperture Radar

Balzter[1], Heiko, Baker[1], John R., Hallikainen[2], Martti and Tomppo[3], Erkki

[1] Centre for Ecology and Hydrology, Section for Earth Observation, Monks Wood, Abbots Ripton, Huntingdon, Cambridgeshire, PE28 2LS, UK
[2] Helsinki University of Technology, Laboratory of Space Technology, Otakaari 5 A, FIN-02150 Espoo, Finland
[3] Finnish National Forest Inventory, Finnish Forest Research Institute, Unioninkatu 40 A, FIN-00170 Helsinki, Finland

Abstract

Airborne polarimetric Synthetic Aperture Radar (SAR) is used for estimating stem volume of a Finnish boreal forest by comparing different empirical models. Its capability for retrieval of snow water equivalent is then explored. Fully polarimetric L- and C-band data were acquired over a Finnish test site in March and May 1995. The information content was explored qualitatively by inspecting polarimetric colour composites, and by applying decomposition algorithms to the polarimetric covariance matrices at individual frequencies. Three families of quantitative models were fitted to estimate stem volume:

1) F1P1 models, using a single frequency and a single polarisation;
2) F2P1 models, using the difference between HV polarisation at C- and L-band related to stem volume;
3) F1P4 models, based on a single frequency and the full polarimetric information, selected by stepwise multiple regression with stem volume;

Stem volume estimates from SAR are compared with digital stem volume data by the Finnish Forest Research Institute. Prior information about the stem volume distribution addresses the saturation problem of the microwave response. The L-band F1P4 models in March and May 1995 have the smallest root mean square (rms) errors, around 22 m^3/ha.

Three multiple regression models to retrieve snow water equivalent from backscatter are presented:

1) EU model, an explorative, uncorrected multiple regression model;
2) EC model, an explorative, stem volume corrected multiple regression model;
3) CC model, a statistically conservative, stem volume corrected multiple regression model.

The accuracy of snow water equivalent estimates was improved significantly by a simple linear correction for stem volume. The statistically conservative CC model showed that only L-band in HH polarisation explained a significant (P<0.05) proportion of snow water equivalent (r^2=0.51). The explorative EC model resulted in r^2=0.68 (P>0.05).

Conclusions are:
1) Decomposition algorithms of the polarimetric covariance matrix result in information on scattering mechanisms in the vegetation canopy and on the ground, so being potentially of great value for land cover mapping;
2) Satellite polarimetric SARs, for example those to be flown on Envisat and ALOS, will be able to estimate stem volume on continental and global scales;
3) L-band SAR has a potential for snow cover mapping and run-off prediction.

Keywords

Finland, WINTEX, decomposition algorithm, carbon, forest mapping, biophysical parameters

1. Introduction

Analysis of the carbon budget implies that there is a net carbon sink in the terrestrial biosphere, with a substantial contribution being required if the budget is to be brought into balance. This contribution could arise from the landmasses of the Northern Hemisphere, although it is not clear whether it is associated with an imbalance in production and decomposition in the deciduous forests at temperate latitudes or from the boreal forests lying at high northern latitudes. The role of boreal forests in the carbon cycle is certainly important, for the CO_2, which they take up and release may account for up to half of the seasonal variation in this component. Moreover the seasonal amplitude of atmospheric CO_2 concentrations in northern latitudes has increased with time. There is increased metabolic activity of ecosystems in northern latitudes due to a warmer drier climate and to higher atmospheric concentrations of CO_2, and experiments with atmospheric general circulation models indicate a significant climatic warming in the Northern Hemisphere at high-latitudes with an associated doubling of atmospheric CO_2 concentrations. But the ecological implications of such changes are not yet fully understood. In some scenarios annual carbon sequestration increases due to a lengthening of the growing season, but in others a higher decomposition rate of soil organic matter and increased periods of frost drought lead to a decrease.

Remote sensing can in principle provide more reliable estimates for some of the terms contributing to the terrestrial carbon budget. Particularly radar remote sensing has the potential to estimate boreal forest biomass on continental and global scales. Synthetic Aperture Radar (SAR) used for forest monitoring operates at wavelengths of around 5.6 cm (C-band), 24 cm (L-band) and 50 cm (P-band). The utility of imaging radars for investigating terrestrial ecosystems has been reviewed by Kasischke *et al.* (1997) who concluded, *inter alia*, that:
(i) Multichannel radar data, because of their sensitivity to variations in the structure of the vegetation canopy and the moisture of the vegetation and ground layers, provide a means to classify land-cover patterns and detect changes of land cover;
(ii) Imaging radars have the capability to estimate woody plant biomass and thereby monitor biomass variations in forested ecosystems, best performance being achieved with a cross-polarised sensor (HV) at a low frequency (L- or better P-band) (although they do note that this capability varies depending on the forest type, for example with the SIR-C radar the upper levels of sensitivity lie between 100 $t \cdot ha^{-1}$ for complex tropical forest canopies up to 250 $t \cdot ha^{-1}$ for simpler forest structures dominated by a single tree species);
(iii) Spaceborne radars like ERS-1 that have been in continuous operation for several years can provide important information on temporally dynamic processes such as changes in the frozen or thawed status of vegetation.

Rignot *et al.* (1994b) used repeated overflights over the Tanana river floodplain in Alaska to map five vegetation types dominated by white spruce, balsam poplar, black spruce, alder/willow shrubs and bog/fen/non-forest vegetation, plus open water. Classification accuracy was investigated as a function of frequency and polarisation, and of forest seasonal state (which included winter/frozen, winter/thawed, spring/flooded, spring/unflooded, and summer/dry conditions). C-band was more useful than L- or P-band for separating forest types and HV the best polarisation. The highest classification accuracy was obtained by combining L-HV and C-HV data acquired in spring as seasonal river flooding receded but before deciduous tree species came into leaf. Rignot *et al.* (1994b) concluded that future spaceborne SAR systems would have limited mapping capabilities when used alone, but in combination would be able to resolve forest types and to separate non-forest areas. In another study Rignot *et al.* (1994a) estimated above-ground dry biomass of forest stands in the Bonanza Creek Experimental Forest, Alaska, from radar data gathered in winter, spring and summer. As expected C-band backscatter showed little sensitivity to biomass but L- and P-band radar backscatter increased by more than 6 dB as biomass increased from 5 to 200 $t \cdot ha^{-1}$. Biomass was predicted from L- and P-band using second-order polynomial regression, and compared to ground data. At P-band the error in predicted biomass was 30% using HV alone, and 20% when HV, HH and VV were used together. At L-band the corresponding errors were a few percent larger. These errors had components arising from the ground data (uncertainties in stand biomass estimates, significant spatial variations in biomass within a stand, and unusual stand conditions following natural disturbances) and from interactions of the radar signal with the complex canopy structure which caused the biomass retrieval curves to be dependent on seasonal and environmental conditions and on observing geometry.

A problem in the deployment of SAR for forest mapping is the saturation of backscatter at low timber volume. Dobson *et al.* (1992) analysed radar responses to forest biomass at P-, L-, and C-band and found an approximately linear response of backscatter with increasing biomass reaching wavelength dependent saturation levels around 200 $t \cdot ha^{-1}$ for P-band and 100 $t \cdot ha^{-1}$ for L-band. In the study of Imhoff (1995) saturation was reached at 100 $t \cdot ha^{-1}$ for P-band, 40 $t \cdot ha^{-1}$ for L-band and 20 $t \cdot ha^{-1}$ for C-band in coniferous and broadleaf evergreen forests. Luckman *et al.* (1998) found saturation at 60 $t \cdot ha^{-1}$ for L-band in tropical forests. For a boreal forest in Canada Ranson *et al.* (1995) observed saturation at 200 $t \cdot ha^{-1}$ using the ratio of LHV/CHV, with a confidence interval of ± 20 $t \cdot ha^{-1}$ at the 95% level. In contrast to these published saturation limits, Baker and Luckman (1999) found that both C- and L-band backscatter at two Swedish test sites saturated at the very lowest biomass. AIRSAR data from Thetford forest in the UK, which has some similarity to the Swedish sites in its biophysical characteristics, had shown the expected relationship between backscatter and biomass density (Baker *et al.* 1994) so the different behaviour of the Swedish sites may arise from the greater roughness of the ground surface or the greater moisture content of the boreal forest. The accuracy of biophysical parameters retrieved from SAR depends considerably on vegetation structure and ground conditions.

Snow mapping is the second application examined in this paper. Different radars, mainly operating at C-band, have been used for this purpose. Guneriussen *et al.* (1996) observed a decrease in ERS-1 backscatter coefficient of 3 dB between dry and wet snow. Koskinen *et al.* (1999) showed that SAR-derived snow cover maps agree well with ground data and are correlated with AVHRR reflectance. Koskinen *et al.* (1997) used multitemporal ERS-1 SAR to map areas fully covered with wet snow, partly melted areas and snow-free areas in northern Finland. Guneriussen (1997) found that ERS-1 SAR backscatter coefficient decreased linearly as a Landsat TM derived snow ratio increased. Baghdadi *et al.* (1999) propose a radar backscatter model that simulates backscatter from a multi-layer snowpack for various snow cover conditions and for SAR parameters specific to Radarsat (C-HH). Results for Quebec show negligible errors

for wet snow with liquid water content higher than 4%. Below this threshold, the estimation error increases rapidly, and 1% is the required minimum. Underestimation of dry snow cover also was a problem in the SIR-C/X-SAR project by Albright *et al.* (1998). A study of airborne C-band SAR confirmed that scattering from a shallow dry snow cover (snow water equivalent < 20 cm) is undetectable (Bernier and Fortin 1998). Based on SIR-C/X-SAR images, Shi and Dozier (1997) presented a classification algorithm for discriminating dry and wet snow using a DEM, and a second algorithm for mapping wet snow without requiring a DEM. Shi and Dozier (1995) developed an algorithm for retrieving snow wetness from SIR-C/X-SAR based on a first-order scattering model and retrieved snow wetness within a confidence interval of 2.5% wetness. A modelling study of the response of radar to snow at C- and X-band has been carried out by Kendra *et al.* (1998). JPL-AIRSAR at C-band was used for snow mapping with an accuracy exceeding 80% by Shi *et al.* (1994). Baghdadi *et al.* (1998) found that airborne C-HV SAR backscatter could be used for mapping land-cover types at a test site in Canada, despite the presence of wet snow. A snow map derived from ERS-1 SAR has been used for runoff modelling during a full period of snowmelt by Baghdadi *et al.* (1997). Repeat-pass interferometric coherence of two ERS-1/2 SAR images has provided a more reliable way of discriminating wet snow cover (Strozzi *et al.* 1999).

Radar response to snow at L-band has rarely been examined. Comparing JERS-1 L-HH with ERS-1 C-VV imagery, Pulliainen *et al.* (1999) show that the radar response to biomass in a boreal forest is more sensitive to snow at C-band than at L-band. The literature suggests that C-VV shows the best relation with snow. C-HV is less sensitive to snow cover and L-band has been found robust against snow conditions.

This study is part of the European-funded NOPEX / WINTEX (Northern Hemisphere Climate Processes Land Surface Experiment / Winter Experiment) project, in the sub-area of "Land-surface-atmosphere interactions in a winter-time boreal landscape". It aimed to help to meet the objectives of the International Geosphere-Biosphere Programme (IGBP), the World Climate Research Programme (WCRP) and the Human Dimensions of Global Climate Change Programme (HDP). The project philosophy is based on the hypothesis that climatic change has its largest influence at high latitudes and during winter time. The main objective of NOPEX was to study the annual and daily cycles of the regional land-surface budgets of energy, water, and CO_2 by using mesoscale atmospheric models, field data, and hydrological models including dynamics of snow and frozen soils.

The present study focuses on an evaluation of SAR remote sensing techniques to describe aspects of the NOPEX winter-time landscape by investigating the capabilities of SAR for boreal forest inventory under snow conditions. The main interest was originally concentrated on the mapping of snow properties although this was in fact found to be extremely difficult in forested areas (Hallikainen *et al.* 1997). Two objectives were set:

- to estimate total forest stem volume from polarimetric SAR and assess its accuracy
- to study the effects of dry and wet snow on the capabilities of SAR for boreal forest inventory.

2. Material and methods

2.1. Study site

The test site Pikkarala is the second of four snow test sites from the EMAC95 campaign. It is located in the south of Finnish Lapland (Figure 1), bounded by 64°50'38" N 25°39'02" E (upper left) and 64°53'45" N 25°48'14" E (lower right). It extends along the left bank of the river Oulujoki which flows into the Gulf of Bothnia to the north-west at the city of Oulu. The test site

consists of mineral soil, spruce and mires and open bogs, and has a large proportion of productive forest land. The most common tree species is pine (*Pinus silvestris* L.) with spruce (*Picea abies* (L.) Karsten), birch (*Betula spp.)* and other broad leafed tress as minority.

[insert Figure 1 about here]

2.2. SAR data

Airborne SAR data were acquired during the European Multi-sensor Airborne Campaign (EMAC-94/95) by the EMISAR sensor of the Technical University of Denmark (TUD). Characteristics of EMISAR are given in Attema and Wooding (1994).

EMISAR has fully polarimetric capabilities. All images were lowpass filtered, resampled to 5 m pixel spacing and radiometrically calibrated. Ground control points from 1:20 000 topographic maps were used to geocode the images to the Finnish national grid, with a first-order model and nearest neighbour resampling. The backscatter images were averaged over a 20 by 20 pixel window for the stem volume estimation.

EMISAR measures the covariance matrix of the target for each pixel.

$$C = \begin{bmatrix} < S_{HH}.S_{HH}^* > & < S_{HH}.S_{HV}^* > & < S_{HH}.S_{VV}^* > \\ < S_{HV}.S_{HH}^* > & < S_{HV}.S_{HV}^* > & < S_{HV}.S_{VV}^* > \\ < S_{VV}.S_{HH}^* > & < S_{VV}.S_{HV}^* > & < S_{VV}.S_{VV}^* > \end{bmatrix} \quad (4)$$

Assuming that targets exhibit reflection symmetry about a plane perpendicular to the line of sight, which is likely to be true for natural targets, then the co-polarised and cross-polarised terms are uncorrelated (Borgeaud *et al.* 1987):

$$C = \begin{bmatrix} < S_{HH}.S_{HH}^* > & 0 & < S_{HH}.S_{VV}^* > \\ 0 & < S_{HV}.S_{HV}^* > & 0 \\ < S_{VV}.S_{HH}^* > & 0 & < S_{VV}.S_{VV}^* > \end{bmatrix} \quad (6)$$

Thus *C* has been reduced from a four by four complex matrix to five numbers: three real numbers, namely the powers returned in the two co-polarised and one cross-polarised configurations, $<S_{HH}.S_{HH}^*>$, $<S_{VV}.S_{VV}^*>$ and $<S_{HV}.S_{HV}^*>$, further denoted as HH, VV and HV, and one complex number, the cross-correlation of the horizontal and vertical polarisations $<S_{HH}.S_{VV}^*>$ abbreviated as HHVV*. From the off-diagonal term of the covariance matrix, the intensity of HHVV* and the phase Φ can be determined. These parameters are physically related to the scattering order and the dielectric properties of the target. Freeman and Durden (1998) and Cloude and Pottier (1996, 1997) make further use of the covariance matrix in their decomposition algorithms.

Freeman and Durden (1998) present a three-component scattering model for polarimetric SAR data. The covariance matrix is used to attribute backscatter to three basic scattering mechanisms: canopy scatter from a cloud of randomly oriented dipoles, double-bounce scatter from a pair of orthogonal surfaces with different dielectric constants and Bragg scatter from a moderately rough surface. Cloude and Pottier (1996, 1997) propose an entropy-based classification scheme for polarimetric SAR data. The derived entropy and an angle α can be used to classify polarimetric SAR images into typically nine zones. α is an angle between 0° and 90° according to the predominant scattering mechanism, corresponding to surface scattering in the geometrical

optics limit (α=0°), and to successively surface scattering under physical optics, the Bragg surface model, dipole scattering, double bounce scattering and dihedral scattering from metallic surfaces (α=90°). The entropy is a smoothly increasing function of scattering order as depolarisation increases. For high scattering orders almost random noise is the result, corresponding to the entropy approaching unity. α increases with scattering order too, approaching 60° in the limit. This is only valid if HV is uncorrelated with HH and VV. For 100 m pixel spacing this assumption is likely, but it would probably not be valid for some targets at the original high resolution of 3 m (Cloude, personal communication).

2.3. Ground data

Surrogate forest ground data were provided by the Finnish National Forest Inventory (FNFI), Finnish Forest Research Institute (FFRI.). Stem volume was provided by tree species in increments of 2 m^3/ha on a 25 m grid. It is directly related to forest dry biomass by the equation (Pulliainen *et al.* 1994):

$$M_B = c \cdot \rho_d \cdot Vol \qquad (1)$$

where M_B is the biomass in $t \cdot ha^{-1}$, c is a proportionality constant depending on the structural forest type and lies in the range 1.4 to 2.1, ρ_d is the density of dry wood in t/m^3 (around 0.4 for pine), and *Vol* is the tree stem volume in m^3/ha.

FFRI estimated the stem volume from 1992-1993 Landsat 5 Thematic Mapper images and field measurements. The techniques are described by Tomppo (1997) and consists of systematic clusterwise sampling, feature selection and *k* nearest neighbour estimation. The total growing stock volume in Finnish forests in 1989-94 was 1.94 billion m^3 with a relative standard error of 0.6% (Tomppo and Henttonen 1996). The standard error for an area of one million hectares is around 1-2%. At a pixel level of 25 m by 25 m the relative standard error of the multi-source inventory is as high as 60 %, but decreases rapidly with increasing area (Tomppo 1997).

To predict stem volume from backscatter the digital stem volume map was averaged over a four by four window to a 100 m grid. A mask of forested areas was created from the digital stem volume map, mixed forest and non-forest pixels being treated as non-forest. The mean stem volume is 50.5 m^3/ha. The type I error probabilities in all statistical analyses are denoted as P. A statistical test is considered significant if P<0.05.

For the retrieval of snow water equivalent, snow fork measurements were carried out by the Helsinki University of Technology (HUT) at the test site Pikkarala along a track of 9200 m length from 64°50.60' N, 25°39.42' E to 64°53.87' N, 25°48.70' E. Over homogeneous areas near points 1 km apart. measurements were made of snow depth, permittivity, wetness and density on each of five days, 22/3, 4/4, 5/4, 2/5 and 3/5/1995 (Hallikainen *et al.* 1997). From the processed EMISAR data SAR backscatter intensities were averaged over a five by five pixel window onto a 25 m grid. Bitmap masks of ten homogeneous areas around the snow fork sampling points were delineated and the mean stem volume per area, mean backscatter intensities and mean snow parameters under the masks were extracted.

2.4. Stem volume estimation

The forest pixels were divided into two random samples of 1849 and 5547 pixels. Model parameters were estimated from sample 1, and stem volume was predicted from sample 2, calculating accuracy statistics at the same time. The root mean square error is defined as

$$rmse = \sqrt{\frac{\sum (y_{obs} - y_{pred})^2}{n - k}} \qquad (8)$$

where y_{obs} = observed value, y_{pred} = predicted value, n = number of observations, and k = number of model parameters. The relative standard error (s_e), also termed the 'relative accuracy' by Hyyppä *et al.* (1997), is defined as rms error divided by the mean prediction (Tokola *et al.* 1996) and remarkably this implies that a strong positive bias (overestimation of stem volume) decreases s_e. The four parameters rmse, s_e, Pearson's correlation coefficient (r) and bias were calculated from predicted and observed stem volume in m^3/ha.
Outliers in the curves were eliminated using the linear relation between standard deviation of backscatter and mean stem volume. Stem volume retrieval from the SAR data was carried out using three types of models:

- F1P1 models using one frequency and one polarisation. An exponential model described backscatter as a function of stem volume. It provides information on scattering contributions to the backscatter (Pulliainen *et al.* 1996).
  $$\sigma^0 = a - e^{-(b \cdot Vol + c)} \quad (7)$$
  where a is the saturation level, b describes the shape of the curve, and c the backscatter at zero stem volume compared to the backscatter at saturation.
  Information about forest pixels with high stem volume above the saturation, is obtained from sample 1. Stem volume of these pixels is normally distributed for all wavelengths and polarisations. Mean μ_{Vol} and standard deviation σ_{Vol} of all normal distributions are estimated from all pixels above the saturation level. A random sample is drawn from this distribution in this case to get a predicted stem volume. To estimate stem volume from the model three cases were distinguished:
  1) if $\sigma^0 \le a - e^{-c}$ predict $Vol = 0$;
  2) if $\sigma^0 > a - e^{-c}$ and $\sigma^0 < a$ predict $Vol = \frac{c + \ln(a - \sigma^0)}{-b}$;
  3) if $\sigma^0 \ge a$ predict $Vol \sim N(\mu_{Vol}, \sigma_{Vol})$.
- F2P1 models using two frequencies and one polarisation. An exponential curve was fitted to the difference of C-HV and L-HV backscatter coefficients (dB) and the stem volume.
  $$\sigma^0_{CHV} - \sigma^0_{LHV} = a + e^{-(b \cdot Vol + c)} \quad (9)$$
- F1P4 models using one frequency and four polarisations, HH, VV, HV and HHVV*. After a logarithmic transformation stem volume showed a linear relationships with backscatter coefficients for most frequencies and polarisations (in this transformation zero stem volumes were substituted by 1 m^3/ha to avoid infinite values). The Efroymson algorithm of stepwise regression model selection (Miller 1984) was used to determine the significant regressors in the model.

2.5. Snow parameter retrieval

Snow water equivalent is the integral of the snow density through the snow pack. The backscatter coefficient was corrected for stem volume by linear regressions. Three stepwise regressions were carried out:

- EU model: In the explorative uncorrected (EU) model the equation included backscatter at all frequencies and polarisations, without testing their statistical significance. The backscatter coefficient was not corrected for variations in stem volume.
- EC model: The explorative, stem volume corrected (EC) model also includes all frequencies and polarisations without statistical tests.
- CC model: The statistically conservative, stem volume corrected (CC) model uses only statistically significant backscatter terms in the equation.

Stem volume correction was based on simple linear regressions of backscatter coefficient and total stem volume in the area around the measurement points from the snow experiment. The

corrected backscatter coefficient is defined as the residual backscatter (difference between measured backscatter and the fitted line).

3. Results

3.1. Polarimetric covariance matrix

Figure 2 shows a colour composite of test site Pikkarala for the L-band data acquired by EMISAR on 2 May 1995. The image is geocoded to the Finnish national grid, with a superposed 1 km grid, and red, green and blue correspond to HV-, VV- and HH polarisations. Figure 3 shows four different representations of the L-band data for an area of interest (7201.00 N, 3440.00 E to 7196.25 N, 3444.75 E). The information in these four representations is complementary, e.g. the airfield in the north-west corner. In Figure 3a the presentation is the same as Figure 2, while in Figure 3b red, green and blue are derived from a transformation of intensity, hue and saturation, using the intensity and phase of HHVV* (and a constant saturation). Agricultural fields appearing green in the HV, VV, HH representation appear bright yellow in the HHVV* representation corresponding to a low scattering order with low depolarisation but high received power. Black fields in Figure 3a also show a low depolarisation, but accompanied by a low intensity, taking a brownish colour in Figure 3b. Over the forested area the phase difference has a large variation due to multiple scattering events.

[insert Figures 2 and 3 about here]

Figure 3c shows the basic scattering mechanisms using the decomposition of Freeman and Durden (1998), and that of Cloude and Pottier (1996, 1997). In the Freeman and Durden decomposition the pink and yellow forests emerge as red as a consequence of the high volume scattering in the crowns, agricultural fields are dominated by surface scattering and appear green (the direction of ploughing has an effect on the radar illumination of these fields) and man-made targets such as buildings cause double-bounce scattering and appear blue. In the Cloude and Pottier decomposition water and very smooth surfaces have a low entropy corresponding to a high degree of order while scattering from a cloud of particles, like water droplets in leaves in a forest or vegetation with highly anisotropic scattering elements, have a high entropy corresponding to a high degree of disorder so that forest appears bright and agricultural land dark. Forest cause multiple scattering events in the crown volume, resulting in high disorder or entropy of the backscattered waves, and ultimately in forests appearing bright, α values around 45° being characteristic of high entropy vegetation scattering. Agricultural fields appear from green to dark blue, due to lower or higher α respectively. Low α indicates some surface scattering mechanism, which is often combined with low entropy resulting in dark green, while dark blue indicates high α and low entropy pointing to multiple scattering events provided for example by isolated dielectric dihedral scatterers. The Cloude decomposition yields complementary information compared to the other representations in Figure 3 and the decomposition parameters entropy and α may be useful for discrimination between forest and non-forest. After this descriptive and qualitative inspection of the images, a more quantitative analysis of the data concludes the study.

3.2. Backscatter and stem volume

A model from Ranson *et al.* (1997) uses a linear relationship between the cube root of stem volume and the backscatter coefficient. This model is less intuitive than the exponential model but does not saturate at high stem volume. The cube root model has been tested for the Pikkarala data and resulted in smaller rms errors than the exponential model, but the error structure

revealed that it tended towards overestimation of low stem volume and underestimation of high stem volume. The focus here lies on the exponential models.

3.2.1. F1P1 models

Figure 4 shows the F1P1 models in March 1995, and Figure 5 in May 1995. For L-band L-HV (March) is most closely related to stem volume. For C-band C-HH and C-HV backscatter show strong relations to stem volume in March but not in May. Snowmelt can explain the increase in backscatter for C-HV and C-HH between March and May for pixels with low stem volume. From visual observations it is known that in March the tree crowns in areas with high stem volume (>50 m^3/ha) were partly covered with relatively dry snow, whereas they were snow-free in areas with lower stem volume, while in May all tree crowns were snow-free. There is little difference in C-band between March and May in areas of high stem volume, because scattering in C-band occurs mainly in the crown. The dry snow in the tree crowns in March has a very low dielectric constant and does not change C-band backscatter much. In May the thickness of the snow layer on the ground varied substantially depending on the stem volume. In areas with high stem volume the thickness of the snow layer was up to 35cm, whereas in areas of low stem volume the thickness was less than 10 cm and non-forested areas were mostly snow free. Consequently C-band backscatter in areas with low stem volume is stronger (Figure 5), because a larger proportion of the ground contributes to it, and wet soil has a high dielectric constant. Figure 6 shows the differences in backscatter between the March and May acquisitions. L-band shows a consistent difference in backscatter between March and May but is related to stem volume at both dates (Figure 5).

[insert Figure 4, 5and 6 about here]

The accuracy assessment in Table 1 shows that L-HV has the smallest rms error, and its predictions are highly correlated with the observations (r_{March}=0.63, r_{May}=0.68). Predictions derived from a normal distribution for pixels where the radar signal has saturated are shown as 'plus' symbols. Rms error increased non-linearly for high stem volume above a frequency and polarisation dependent threshold (around 70 m^3/ha for L-HV). L-HH gives similar results.

[insert Table 1 about here]

The saturation of the backscatter signal limits the applicability of SAR radiometry to forest biomass estimation. The number of pixels within the predictable range is determined by the saturation parameter, a, and the intersection with the backscatter axis, $a-e^{-c}$. In this study, as in many others (section 1), curves in C-band generally saturate more quickly than in L-band.

3.2.2. F2P1 models

Figure 7 shows the relationship between the C–HV and L–HV difference and stem volume in March and May. In test site Pikkarala only the May acquisition shows a relationship to stem volume (Figure 7). Saturation of this model is reached at higher stem volume than for the F1P1 models. A comparison of stem volume predictions with observations for sample 2 reveals a higher rms error, but the lowest bias of all models (Table 1). The stem volume dependent dynamic changes in C-HV backscatter from March to May and from dry to wet snow conditions change the scatterplot significantly (Figure 7).

[insert Figure 7 about here]

3.2.3. F1P4 models

The stepwise regressor selection resulted in the four linear models:

L-band, March: $\log(Vol) = 3.43 + 0.1917 \cdot \sigma^0_{HV} - 0.12 \cdot \sigma^0_{VV} - 0.03 \cdot \sigma^0_{HHVV*}$

L-band, May: $\log(Vol) = 2.71 + 0.03 \cdot \sigma^0_{HH} + 0.11 \cdot \sigma^0_{HV} - 0.03 \cdot \sigma^0_{VV} - 0.05 \cdot \sigma^0_{HHVV*}$

C-band, March: $\log(Vol) = 3.55 - 0.14 \cdot \sigma^0_{HH} + 0.16 \cdot \sigma^0_{HV} + 0.08 \cdot \sigma^0_{VV} - 0.03 \cdot \sigma^0_{HHVV*}$

C-band, May: $\log(Vol) = 3.85 - 0.11 \cdot \sigma^0_{HH} + 0.23 \cdot \sigma^0_{HV} - 0.03 \cdot \sigma^0_{VV}$

The signs of the regressors in these equations are consistent for all polarisations in L-band and for all except VV polarisation in C-band. C-band backscatter for the May acquisition shows the strongest underestimation of high stem volume. The results of the accuracy assessment in Table 1 confirm that it shows the worst fit of the four F1P4 models, having the highest rms error, highest bias and lowest correlation coefficient. As temperatures rise above zero and snowmelt begins, the F1P4 model in C-band loses accuracy (Table 1). However, polarimetric SAR at L-band can be used to map stem volume regardless of snow cover. The rms errors of the L-band F1P4 models in March and May are only slightly different (21.6 and 22.1 m^3/ha). Although the F1P4 model is still biased the use of the full polarimetric information reduces the rms error (Table 1).

3.3. Retrieval of snow water equivalent from SAR

Visual interpretation of the relationships between backscatter, stem volume and snow cover indicated the following trends in the data (Figure 8):

- At L-band backscatter is consistently greater in May than in March (red vs. blue points). In May snow water equivalent was less than in March (size of the points).
- The typical increase of L-band backscatter with stem volume was not lost through changing snow properties.
- For C-band no consistent trend between March and May was observed. The greater snow water equivalent apparently reduces the backscatter in stands with low stem volume.
- The lower the stem volume the greater the variation in backscatter caused by different snow water equivalent.

Numerical analyses revealed the following regression equation for the EU model:

$$SW = -0.37 + 1.01 \cdot \sigma^0_{LHH} - 0.94 \cdot \sigma^0_{LVV} - 1.13 \cdot \sigma^0_{LHV} - 1.68 \cdot \sigma^0_{CHH} + 1.11 \cdot \sigma^0_{CVV} + 1.32 \cdot \sigma^0_{CHV}$$

where SW is the snow water equivalent (g/cm^2) and the σ^0 are the backscatter coefficients (dB) for each frequency and polarisation. This model explains only 34% of the variance of snow water equivalent (r^2=0.34). The results of the explorative model after correction for stem volume variation (EC model, see Table 2) are shown in Figure 9. The EC model explains 68% of the variance of snow water equivalent (r^2=0.68):

$$SW = -41.37 + 0.15 \cdot \sigma^0_{LHHc} + 1.54 \cdot \sigma^0_{LVVc} - 2.54 \cdot \sigma^0_{LHVc} - 2.27 \cdot \sigma^0_{CHHc} - 1.46 \cdot \sigma^0_{CVVc} + 1.73 \cdot \sigma^0_{CHVc}$$

where σ^0 are now the corrected backscatter coefficients (dB) for each frequency and polarisation.

[insert Table 2 and Figure 8 about here]

Statistical tests of the slope parameters of the EC model revealed that only the corrected L-HH backscatter was significant. This is the only term included in the CC model:

$$SW = -26.14 - 2.14 \cdot \sigma^0_{LHHc}$$

In the CC model (r^2 = 0.51) the corrected L-HH backscatter coefficient for SW=0 is –12.2 dB, and as SW rises the backscatter drops to –16.8 dB.

[insert Figure 9 about here]

L-HH is identified by the CC model as the only backscatter component, which is statistically related to snow water equivalent. L-band is known to penetrate dry snow, and has therefore not been considered for snow mapping before. The relation to snow water equivalent is due to the fact that the snow layer was slightly wet in March and even wetter in May, the decrease of L-HH backscatter coefficient with increasing snow water equivalent being caused by increasing attenuation in the snow layer (the attenuation increases with wetness and depth of the snow layer, and depth is related to snow water equivalent). This hypothesis was tested by a linear regression of L-HH backscatter on stem volume, snow wetness (% weight) and snow water equivalent. The results show that stem volume ($P<0.001$) and snow wetness ($P=0.011$) explain 93% of the variance of L-HH backscatter ($r^2=0.93$) but that snow water equivalent is not contributing significantly to this ($P>0.05$).
Further investigations have been carried out on the relation between snow and C-band backscatter. Three multiple linear regressions between C-HH, C-VV and C-HV backscatter and stem volume, snow wetness (% weight) and snow water equivalent were calculated. 93% of the variance of C-VV ($r^2=0.93$) and 88% of C-HV ($r^2=0.88$) could be explained by stem volume, but there was no significant influence from the two snow variables ($P>0.05$). But stem volume, snow wetness and snow water equivalent (all $P<0.05$) explained 80% of the variance of C-HH backscatter ($r^2=0.80$). However prediction of snow water equivalent from stem volume corrected C-HH backscatter was impossible because the slope of the regression line was not significant ($P>0.05$). The difficulties to find statistically significant relationships could be overcome by increasing the sample size. The analysis here should be seen as an exploratory assessment of the potential usefulness of airborne polarimetric SAR for snow studies, the explanation of 51% to 68% of the variance of snow water equivalent justifying further research into the use of L-band SAR for the mapping of wet snow.

4. Discussion

4.1. Stem volume

Monitoring of boreal forests on continental or global scales requires remote sensing techniques. Stem volume can be estimated from quad-polarised L-band SAR with reasonable accuracy. At the Finnish test site Pikkarala, which represents a low biomass high latitude boreal forest, there was a consistent relationship between L-HV and L-HH backscatter and stem volume at both acquisition dates. The saturation of the signal implied that even for L-HV 11%-15% of pixels were outside the dynamic range of the model. C-band only shows a dependence on stem volume in March, but not in May.

Comparing the backscatter coefficients from March and May, wavelength- and polarisation-dependent shifts of the dynamic range and the saturation level were observed due to effects of changing conditions of the targets. The snowmelt resulted in snow-free areas and areas with wet, dense snow in May. At L-band a consistent shift by about 4 dB was observed (Figure 6), but at C-band only the backscatter of some plots with low stem volume changed markedly. This is explained by the wavelength-dependence of the dominant scattering mechanism and the change in snow cover in the tree crowns and on the ground.

The lowest rms error of all examined models was found for the L-band F1P4 models in March (rmse=21.6 m^3/ha) and May (rmse=22.1 m^3/ha). The F2P1 suggested by Ranson *et al.* (1995) were very sensitive to snow. The true rms error of stem volume retrieval from polarimetric SAR is likely to be smaller than the values stated here, because the surrogate ground data are estimates from Landsat TM5 imagery and sparse field sample plot data. Standwise instead of pixelwise stem volume estimation would further reduce the rms error. Nevertheless, the estimates are more accurate than from multi-temporal ERS-1 SAR (Pulliainen *et al.* 1996), Landsat TM (Tokola *et*

al. 1996, Hyyppä *et al.* (1997), and SPOT (Tokola *et al.* 1996). This partly reflects the higher resolution of EMISAR compared to spaceborne platforms. At other test sites in Finland Pulliainen *et al.* (1996) obtained rms errors in the range of 87 - 98 m^3/ha (s_e=0.45 - 0.56) and bias between 0 and 7 m^3/ha for standwise stem volume estimation from 23 multitemporal ERS-1 C-VV SAR, images, sample plot information and a semi-empirical backscatter model. Hyyppä *et al.* (1997) describe a comparison of different remote sensing methods from the literature with their own study of stem volume estimation using data from the helicopter-borne ranging scatterometer instrument HUTSCAT. Hyyppä *et al.* (1997) found that their C-band HUTSCAT ranging scatterometer-based stand level estimates that employ tree height were more accurate (rmse=31.3 m^3/ha, s_e=0.27) than aerial photography (rmse=55.6 m^3/ha, s_e=0.29) and Landsat TM (rmse=84.2 m^3/ha, s_e=0.45), but less accurate than ocular field inventory (rmse=30 m^3/ha, s_e=0.16). Tokola *et al.* (1996) use Landsat TM, Landsat MSS and SPOT imagery to estimate total stem volume at four Finnish test sites with pixel spacings of 20 m and 50 m respectively, with rms errors between 69 and 95 m^3/ha, s_e in the range of 0.62 to 0.85, and bias between -3.7 and 1.1 m^3/ha. The rms error found in this study is smaller, but s_e is greater than that from HUTSCAT, aerial photography and ocular field inventory (Hyyppä *et al.* 1997). This is caused by the fact that the mean stem volume at test site Pikkarala is smaller than that at the test site by Hyyppä *et al.* (1997).

A method of tackling the saturation problem was developed. The use of prior information about the stem volume distribution of pixels above the saturation level proved to be a useful method to avoid severe underestimation of high stem volume.

Despite the limitations of SAR discussed here, it provides a reliable data source for estimating carbon pools in boreal forests because cloud cover and low sun angles do not impede imaging. Because of the saturation of the signal for high stem volume, SAR is particularly useful for mapping sparse and young boreal forests with low stem volume.

The availability of fully polarimetric SAR is still restricted to airborne sensors and the SIR-C mission, which did not cover the boreal region. The launch of Envisat (although twin and not quad polarised) will provide the first spaceborne multi-polarised SAR sensor. For improved stem volume retrieval, the Japanese ALOS mission will be important. ALOS will carry the first operational dual-polarised L-band SAR with an experimental fully polarimetric mode.

4.2. Snow water equivalent

Mapping snow cover is important for hydrological purposes such as assessing snow water equivalent, validation or calibration of hydrological models, run-off prediction and flood warning systems or the inventory of water resources. When the radar illuminates a snow covered area, three scattering mechanisms can be distinguished:

- scattering at the air-snow surface;
- scattering in the snow layer; and
- scattering at the snow-soil boundary.

To understand the scattering behaviour of snow layers cloud models have been used. Volume scattering is related to the proportion of the sizes of the ice crystals to the wavelength. For dry snow e'' is very low and the relative permittivity e'_{ds} is related to snow density and a constant (e'_i of pure ice = 3.15). e'_{ds} under natural conditions is in the range of 1.4 – 2.0. For these parameters most of the incident radiation passes through the boundary. The power reflection from the snow-soil surface is somewhat smaller than from an air-soil surface. The backscatter intensity of dry snow is insensitive to surface roughness of the snow surface. The C-band HH backscatter coefficient has been observed to increase in an exponential function for increasing *SW* of dry snow. At L-band under laboratory conditions dry snow causes less than –20 dB

backscatter for the incidence angle range of EMISAR. Dry snow is difficult to discriminate from a completely snow-free area. Conditions are different for wet snow: Surface roughness changes the backscatter depending on the incidence-angle. The ground contribution becomes less important than for dry snow. For incidence angles above 20 degrees volume scattering is the dominant scattering mechanism. C-HV responds less to wet snow than HH and VV. L-HH does not show differences between wet and dry snow, but C-HH does (about 5 dB in the incidence angle range discussed here). Longer wavelengths are less sensitive to snow wetness, but have a higher detectable range. C-band sensors may thus be expected to have better capabilities to detect the pure presence of wet snow, but longer wavelengths should be better at quantitatively estimating *SW*.

At the test site Pikkarala, snow was drier in March 1995 (0.2-0.5 % liquid water) than in May (>0.8 %). Snow wetness (cv=0.81), snow depth (cv=0.75) and stem volume (cv=0.82) varied more between the snow sampling plots than snow density (cv=0.10). In a previous study of this data by Hallikainen *et al.* (1997) correlations between snow wetness (vol%) and radar backscatter coefficients (dB) were positive ($0.52 < r < 0.75$) for low and negative ($-0.97 < r < -0.83$) for high liquid water content at all wavelengths and polarisations. Hallikainen *et al.* (1997) averaged the backscatter coefficient in square areas of one and nine hectares around the snow fork sampling points. These findings were not confirmed in this study, using visually homogeneous areas instead of squares, and averaging the intensities rather than the backscatter coefficients.

Stem volume is known to mask the effects of snow to some degree (Hallikainen *et al.* 1997), as was confirmed by this study (Figure 8). Based on HUTSCAT airborne ranging scatterometer measurements, the average C-band transmissivity through a boreal (coniferous) forest canopy at an incidence angle of 23° is 0.87 for a stem volume of 50 m^3/ha and 0.76 for 100 m^3/ha respectively (Pulliainen 1994). These values are valid for both horizontal and vertical polarisations and they include the effects of small gaps in the forest. At an incidence angle of 50° as for EMISAR the transmissivity is lower. Recently, the transmissivity has also been determined using airborne microwave radiometer measurements and the result for C-band with vertical polarisation at an incidence angle of 45° was 0.90 for stem volumes of 50 m^3/ha and 100 m^3/ha (Kruopis *et al.* 1999). At L-band the transmissivity is very likely to be greater than 0.90, although no experimental data are available. Thus the effect of stem volume on the backscatter coefficient of snow covered terrain is moderate, but it does have to be accounted for since the dynamic range of the backscatter coefficient itself is only a few dB. The linear correction of backscatter coefficients for stem volume used in the EC model increases the proportion of explained variance of snow water equivalent by 30%. Despite the lack of statistical significance in the EC model, it shows what may be achievable in the future. Additional studies of snow covered forests would be required to validate the findings of this study. Further research on L-band SAR and snow covered forests is justified by the strong interactions between stem volume and snow at C-band which make it hard to explain the observed backscatter. Archived JERS-1 data could be used to validate the empirical relationship found here for spaceborne platforms.

Acknowledgements
This work was funded in part by the NOPEX/WINTEX project within Framework 4 of the European Commission and could not have been undertaken without the full support of the NOPEX Office, particularly Sven Halldin. The aircraft flights were funded by ESA/ESTEC within the EMAC-95 campaign organised by Evert Attema, and flown by the Technical University of Denmark (TUD). We thank Jorgen Dall of TUD for ensuring that the fully polarimetric capabilities of the EMISAR radar were easily accessible to data users and we are grateful to Mike Wooding and Paul Mason of Remote Sensing Applications Consultants (RSAC) for their help with delivery of the EMAC data. We also thank Reija Haapanen and Jari Varjo of

the Finnish Forest Research Institute (FFRI) for providing the forest data, Jaan Praks and Juha Hyyppä of the Helsinki University of Technology (HUT) for supplying the snow data, Kari Leppäaho of the National Land Survey of Finland for sending us the topographic maps, and the Finnish Meteorological Institute (FMI) for providing weather records. Finally, we thank Adrian Luckman, now at the University of Wales at Swansea (UWS) for the use of his C programmes in our image analysis.

References

ALBRIGHT, T. P., PAINTER, T. H., ROBERTS, D. A., SHI, J. C., DOZIER, J., and FIELDING, E., 1998, Classification of surface types using SIR-C/X-SAR, Mount Everest Area, Tibet. Journal of Geophysical Research-Planets, 103, 25823-25837.

ATTEMA, E., and WOODING, M., 1994, EMAC Experimenters Handbook. Programme for 1995.

BAGHDADI, N., FORTIN, J. P., and BERNIER, M., 1999, Accuracy of wet snow mapping using simulated Radarsat backscattering coefficients from observed snow cover characteristics. International Journal of Remote Sensing, 20, 2049-2068.

BAGHDADI, N., GAUTHIER, Y., and BERNIER, M., 1997, Capability of multitemporal ERS-1 SAR data for wet-snow mapping. Remote Sensing of Environment, 60, 174-186.

BAGHDADI, N., LIVINGSTONE, C. E., and BERNIER, M., 1998, Airborne C-band SAR measurements of wet snow-covered areas. IEEE Transactions on Geoscience and Remote Sensing, 36, 1977-1981.

BAKER, J. R., and LUCKMAN, A. J., 1999, Microwave observations of boreal forests in the NOPEX area of Sweden and a comparison with observations of a temperate plantation in the UK, Agriculture and Forest Meteorology, 98, 389-416.

BAKER, J. R., MITCHELL, P. L., CORDEY, R. A., GROOM, G. B., SETTLE, J. J., and STILEMAN, M. R., 1994, Relationships between physical characteristics and polarimetric radar backscatter for Corsican Pine stands in Thetford forest, UK. International Journal of Remote Sensing, 15, 2827-2849.

BERNIER, M., and FORTIN, J. P., 1998, The potential of times series of C-band SAR data to monitor dry and shallow snow cover. IEEE Transactions on Geoscience and Remote Sensing, 36, 226-243.

BORGEAUD, M., SHIN, R. T., and KONG, J. A., 1987, Theoretical models for polarimetric radar clutter. Journal of Electromagnetic Waves and Applications, 1, 73-89.

CLOUDE, S. R., and POTTIER, E., 1996, A review of target decomposition theorems in radar polarimetry. IEEE Transactions on Geoscience and Remote Sensing, 34, 498-518.

CLOUDE, S. R., and POTTIER, E., 1997, An entropy based classification scheme for land applications of polarimetric SAR. IEEE Transactions on Geoscience and Remote Sensing, 35, 68-78.

DOBSON, M. C., ULABY, F. T., LE TOAN, T., BEAUDOIN, A., KASISCHKE, E. S., and CHRISTENSEN, N., 1992, Dependence of radar backscatter on coniferous forest biomass. IEEE Transactions on Geoscience and Remote Sensing, 30, 412-415.

FREEMAN, A., and DURDEN, S. L., 1998, A three-component scattering model for polarimetric SAR data. IEEE Transactions on Geoscience and Remote Sensing, 36, 963-973.

GUNERIUSSEN, T., 1997, Backscattering properties of a wet snow cover derived from DEM corrected ERS-1 SAR data. International Journal of Remote Sensing, 18, 375-392.

GUNERIUSSEN, T., JOHNSEN, H., and SAND, K., 1996, DEM corrected ERS-1 SAR data for snow monitoring. International Journal of Remote Sensing, 17, 181-195.

HALLIKAINEN, M., KOSKINEN, J., PRAKS, J., ARSLAN, A. N., ALASALMI, H., and MAKKONEN, P., 1997, Mapping of snow cover with airborne microwave sensors in EMAC'95. In EMAC 94/95 Final results. Workshop proceedings 14-16/4/1997, ESA WPP-136 (Noordwijk: ESTEC), pp. 143-153.

HYYPPÄ, J., PULLIAINEN, J., HALLIKAINEN, M., and SAATSI, A., 1997, Radar-derived standwise forest inventory. IEEE Transactions on Geoscience and Remote Sensing, 35, 392-404.
IMHOFF, M. L., 1995, A theoretical analysis of the effect of forest structure on Synthetic-Aperture Radar backscatter and the remote sensing of biomass. IEEE Transactions on Geoscience and Remote Sensing, 33, 341-352.
KASISCHKE, E. S., MELACK, J. M., and DOBSON, M. C., 1997, The use of imaging radars for ecological applications - a review. Remote Sensing of Environment, 59, 141-156.
KENDRA, J. R., SARABANDI, K., and ULABY, F. T., 1998, Radar measurements of snow: Experiment and analysis. IEEE Transactions on Geoscience and Remote Sensing, 36, 864-879.
KOSKINEN, J. T., PULLIAINEN, J. T., and HALLIKAINEN, M. T., 1997, The use of ERS-1 SAR data in snow melt monitoring. IEEE Transactions on Geoscience and Remote Sensing, 35, 601-610.
KOSKINEN, J., METSAMAKI, S., GRANDELL, J., JANNE, S., MATIKAINEN, L., and KRUOPIS, N., PRAKS, J., ARSLAN, A., ALASALMI, H., KOSKINEN, J., and HALLIKAINEN, M.T., 1999, Passive microwave measurements of snow-covered forest areas in EMAC'95, IEEE Transactions on Geoscience and Remote Sensing, 37, 2699-2705.
HALLIKAINEN, M., 1999, Snow monitoring using radar and optical satellite data. Remote Sensing of Environment, 69, 16-29.
LUCKMAN, A., BAKER, J., HONZAK, M., and LUCAS, R., 1998, Tropical forest biomass density estimation using JERS-1 SAR: Seasonal variation, confidence limits, and application to image mosaics. Remote Sensing of Environment, 63, 126-139.
MILLER, A. J., 1984, Selection of subsets of regression variables. Journal of the Royal Statistical Society, Series A, 147, 389-425.
PULLIAINEN, J., 1994, Investigation on the backscattering properties of Finnish boreal forests at C- and X-band: A semi-empirical modeling approach, Doctoral thesis, Helsinki, University of Technology, Laboratory of Space Technology, Report 19, 119 pp.
PULLIAINEN, J. T., HEISKA, K., HYYPPÄ, J., and HALLIKAINEN, M. T., 1994, Backscattering properties of boreal forests at the C-bands and X-bands. IEEE Transactions on Geoscience and Remote Sensing, 32, 1041-1050.
PULLIAINEN, J. T., MIKKELÄ, P. J., HALLIKAINEN, M. T. and IKONEN, J. P., 1996, Seasonal dynamics of C-band backscatter of boreal forests with applications to biomass and soil moisture estimation. IEEE Transactions on Geoscience and Remote Sensing, 34, 758-770.
PULLIAINEN, J. T., KURVONEN, L., and HALLIKAINEN, M. T., 1999, Multitemporal behavior of L- and C-band SAR observations of boreal forests. IEEE Transactions on Geoscience and Remote Sensing, 37, 927-937.
RANSON, K. J., SAATCHI, S., and SUN, G. Q., 1995, Boreal forest ecosystem characterization with SIR-C/XSAR. IEEE Transactions on Geoscience and Remote Sensing, 33, 867-876.
RANSON, K. J., SUN, G., WEISHAMPEL, J. F., and KNOX, R. G., 1997, Forest biomass from combined ecosystem and radar backscatter modeling. Remote Sensing of Environment, 59, 118-133.
RIGNOT, E., WAY, J. B., WILLIAMS, C., and VIERECK, L., 1994a, Radar estimates of aboveground biomass in boreal forests of interior Alaska. IEEE Transactions on Geoscience and Remote Sensing, 32, 1117-1124.
RIGNOT, E. J. M., WILLIAMS, C. L., WAY, J. B., and VIERECK, L. A., 1994b, Mapping of forest types in Alaskan boreal forests using SAR imagery. IEEE Transactions on Geoscience and Remote Sensing, 32, 1051-1059.
SHI, J. C., and DOZIER, J., 1995, Inferring snow wetness using C-band data from SIR-C's polarimetric Synthetic Aperture Radar. IEEE Transactions on Geoscience and Remote Sensing, 33, 905-914.
SHI, J. C., and DOZIER, J., 1997, Mapping seasonal snow with SIR-C/X-SAR in mountainous areas. Remote Sensing of Environment, 59, 294-307.

SHI, J. C., DOZIER, J., and ROTT, H., 1994, Snow mapping in alpine regions with Synthetic Aperture Radar. IEEE Transactions on Geoscience and Remote Sensing, 32, 152-158.
STROZZI, T., WEGMULLER, U., and MATZLER, C., 1999, Mapping wet snowcovers with SAR interferometry. International Journal of Remote Sensing, 20, 2395-2403.
TOKOLA, T., PITKÄNEN, J., PARTINEN, S., and MUINONEN, E., 1996, Point accuracy of a non-parametric method in estimation of forest characteristics with different satellite materials. International Journal of Remote Sensing, 17, 2333-2352.
TOMPPO, E. and HENTTONEN, H, 1996. Finnish Forest Resources and their changes since 1951 (in Finnish). Finnish Forest Research Institute. Statistical Bulletin 354. 19 p.
TOMPPO, E., 1997, Application of remote sensing in Finnish National Forest Inventory. In: Kennedy, P.J. Application of Remote Sensing in European Forest Monitoring. International Workshop, Vienna, Austria, 14th - 16th October 1996. Proceedings. Joint Research Centre. European Commission. BOKU. Joanneum Research. p. 375-388

Tables

Table 1. Accuracy assessment of stem volume predicted from the F1P1 model for 100 m pixel spacing. Pearson's correlation coefficient *r* between observations and predictions, root mean square error (rmse), relative standard error (s_e) and bias. Negative bias means underestimation.

model	acquisition date	band and polarisation	*r*	rmse (m^3/ha)	s_e (%)	bias (m^3/ha)
F1P1	March	C-HH	0.26	41.5	62	16.3
F1P1	March	C-HV	0.55	32.0	54	9.1
F1P1	March	C-VV	0.57	31.9	56	6.2
F1P1	March	L-HH	0.54	32.6	55	8.4
F1P1	March	L-HV	0.63	29.1	51	6.2
F1P1	March	L-VV	-	-	-	-
F1P1	May	C-HH	0.23	43.7	65	16.3
F1P1	May	C-HV	0.47	34.6	57	10.5
F1P1	May	C-VV	-	-	-	-
F1P1	May	L-HH	0.62	30.8	57	3.6
F1P1	May	L-HV	0.68	27.5	50	4.3
F1P1	May	L-VV	-	-	-	-
F2P1	May	C-HV - L-HV	0.65	32.3	66	-1.4
F1P4	March	C-HH, VV, HV, HHVV*	0.71	24.5	43	6.6
F1P4	March	L-VV, HV, HHVV*	0.78	21.6	39	4.3
F1P4	May	C-HH, VV, HV	0.58	29.0	48	10.2
F1P4	May	L-HH, VV, HV, HHVV*	0.77	22.1	39	6.0

Table 2. Intercept *a*, slope *b*, and coefficient of determination r^2 of the correction of backscatter coefficients for stem volume by linear regressions.

band and polarisation	*a*	*b*	r^2
L-HH	-14.848	0.0974	59%
L-VV	-15.166	0.0417	13%
L-HV	-23.776	0.1351	48%
C-HH	-12.399	0.0678	45%
C-VV	-13.396	0.0729	69%
C-HV	-20.454	0.1193	79%

Figures

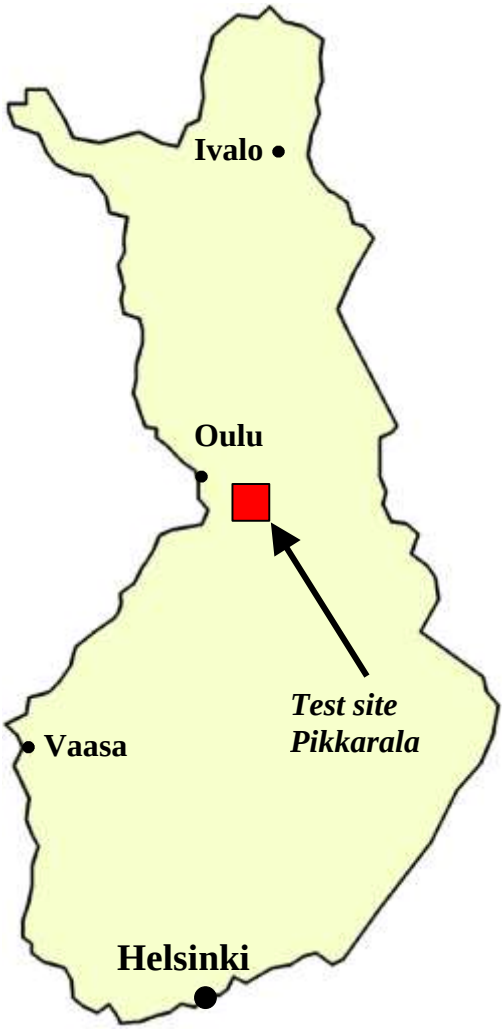

Figure 1. Map of Finland indicating the location of the test site Pikkarala.

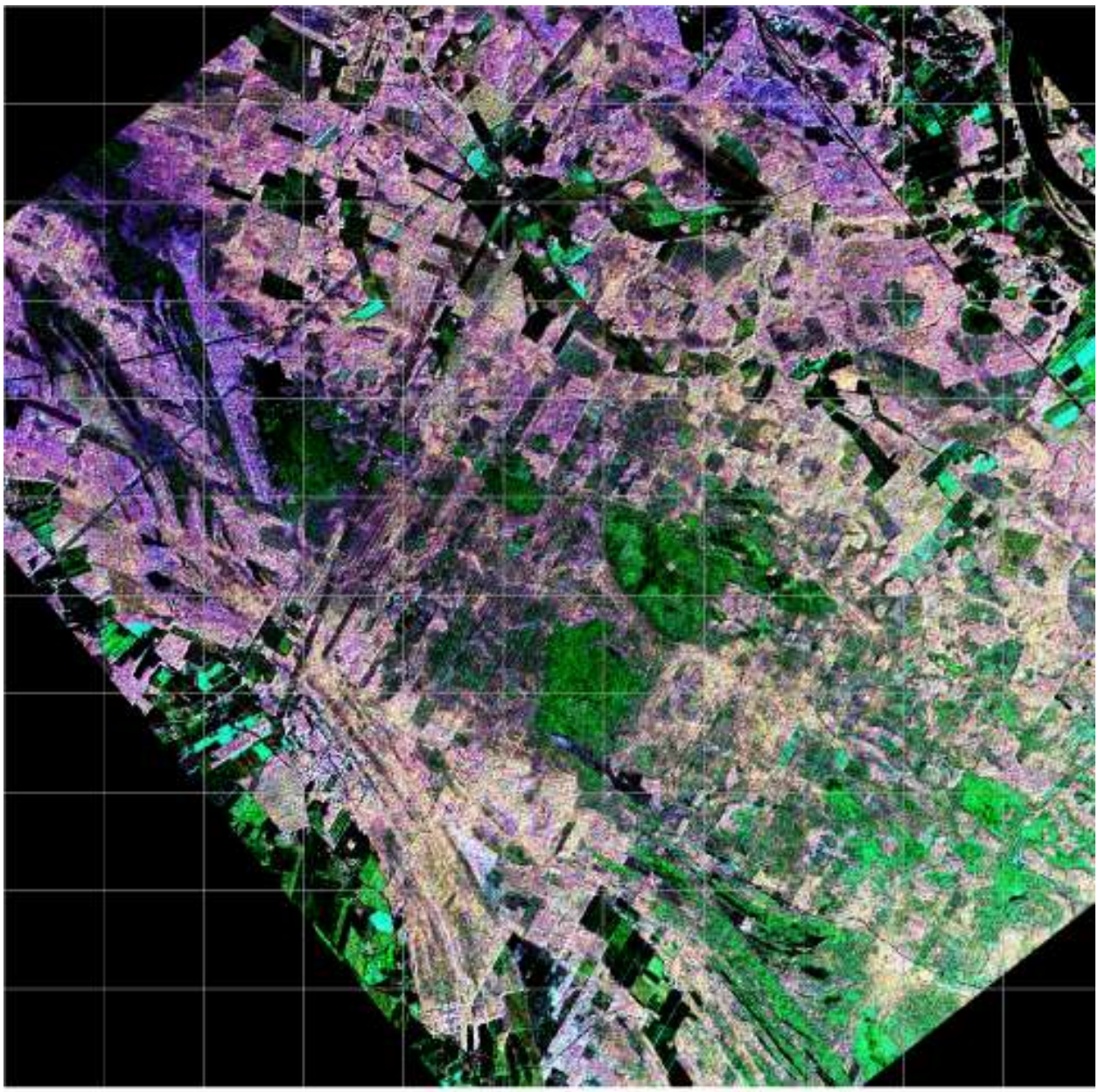

Figure 2. L-Band EMISAR image of the test site Pikkarala acquired on 2 May 1995 and geocoded to the Finnish national grid. The grid spacing is 1 km and red, green and blue correspond to HV-, VV- and HH-Polarisations.

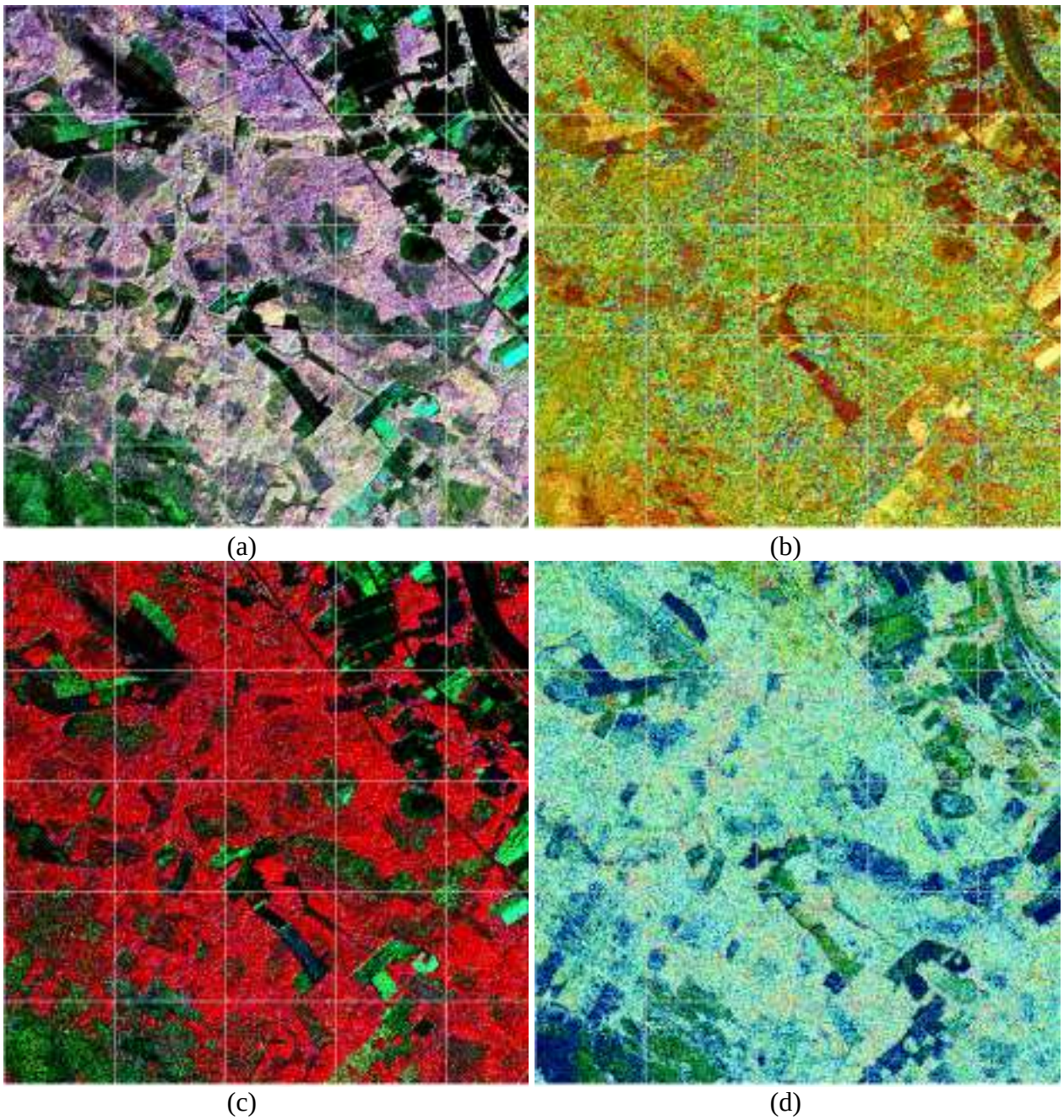

Figure 3. Four representations of the L-Band EMISAR data over part of the test site Pikkarala, acquired on 2 May 1995. Each image is geocoded to the Finnish national grid, with corner coordinates 7201.00 N, 3440.00 E upper left and 7196.25 N, 3444.75 E lower right. The grid spacing is 1 km.
a) Red, green and blue correspond to HV-, VV- and HH-polarisations.
b) Red, green and blue correspond to intensity and phase obtained from HHVV* as intensity and hue.
c) Freeman decomposition. Red, green and blue correspond to power attributed to volume, surface and double-bounce scattering.
d) Cloude decomposition. Red, green and blue correspond to entropy and α as intensity and hue.

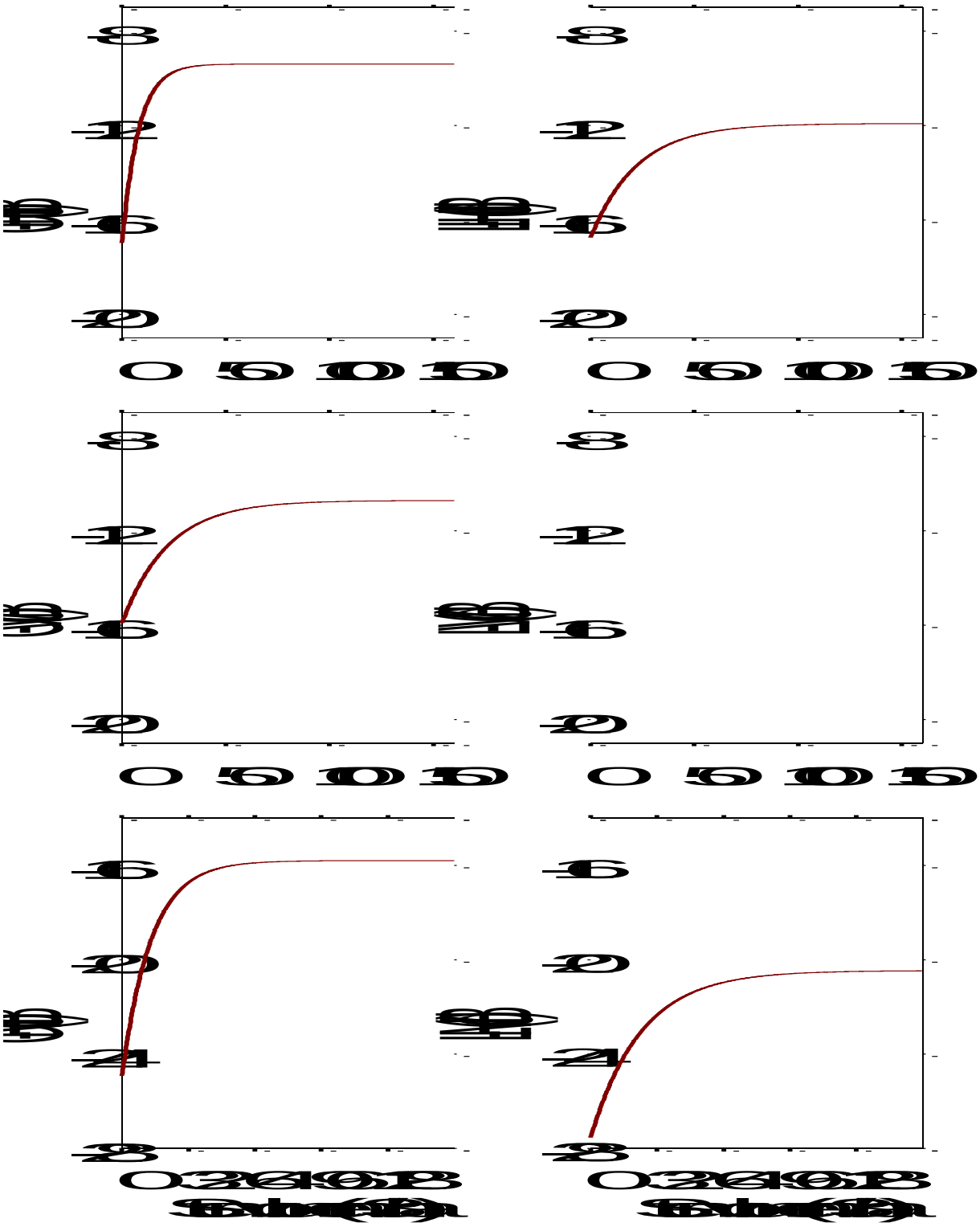

Figure 4. Scatterplots of backscatter coefficients and stem volume with fitted F1P1 models in March 1995.

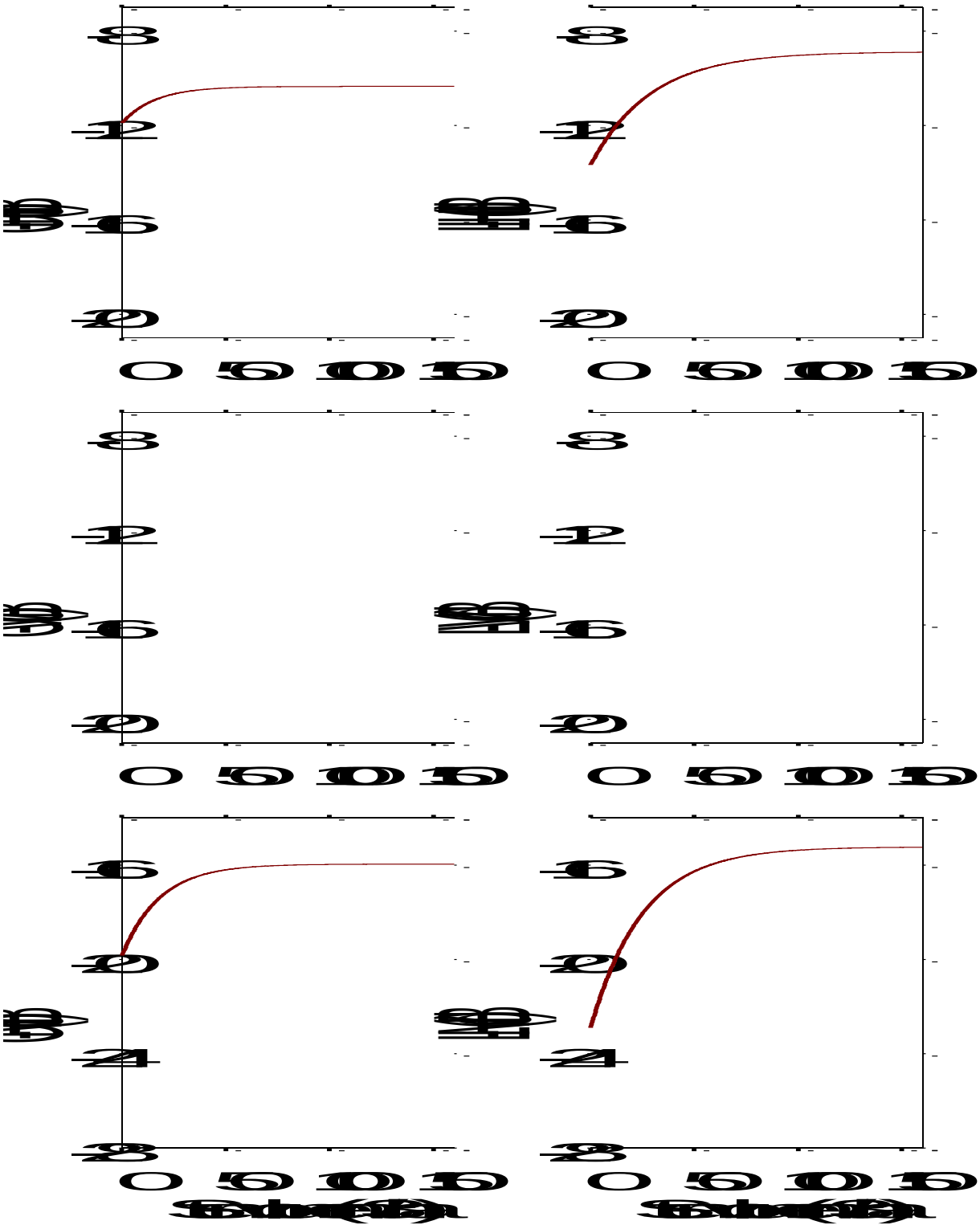

Figure 5. Scatterplots of backscatter coefficients and stem volume with fitted F1P1 models in May 1995.

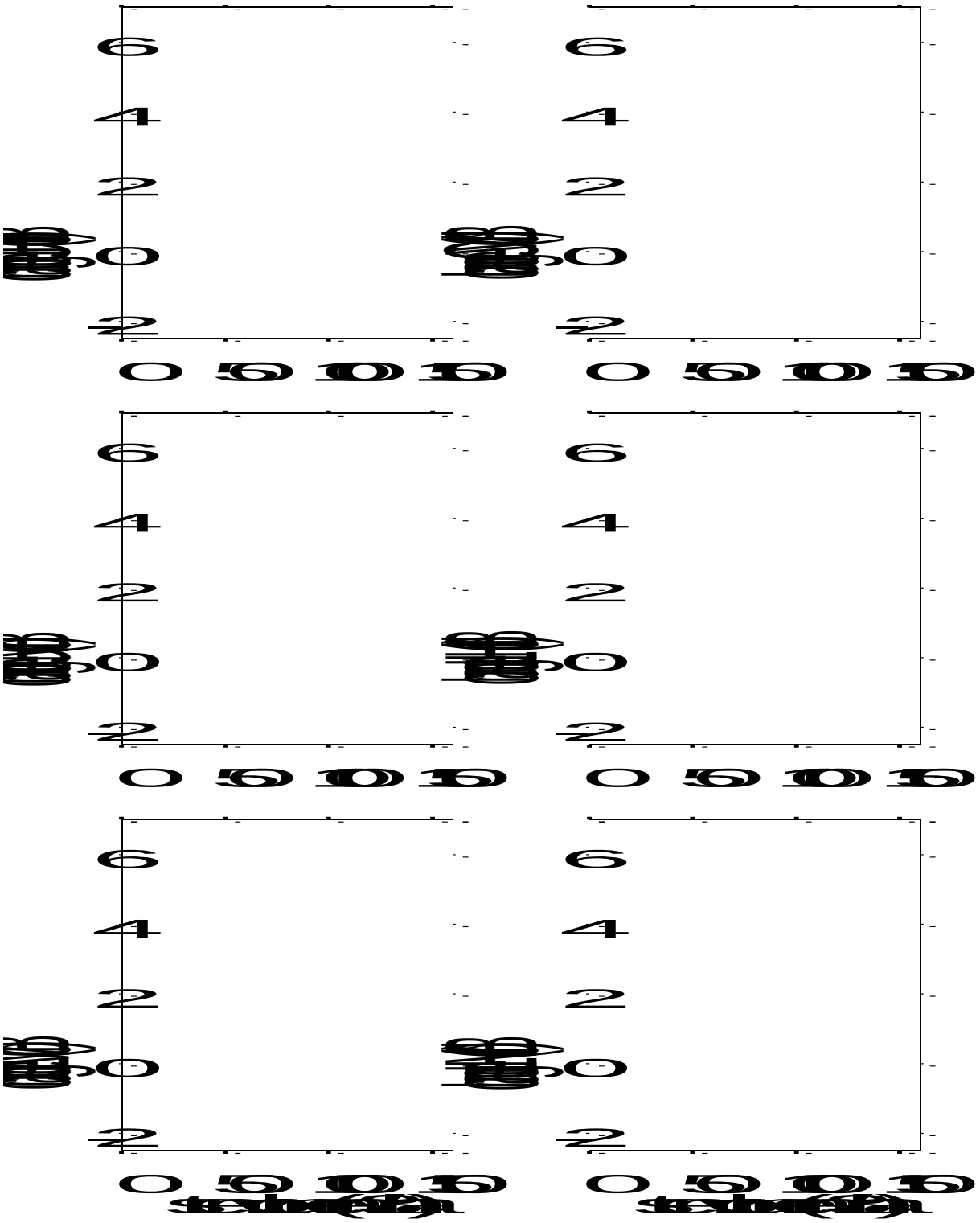

Figure 6. Temporal differences of backscatter coefficients (dB) between March and May. An increase corresponds to a positive sign.

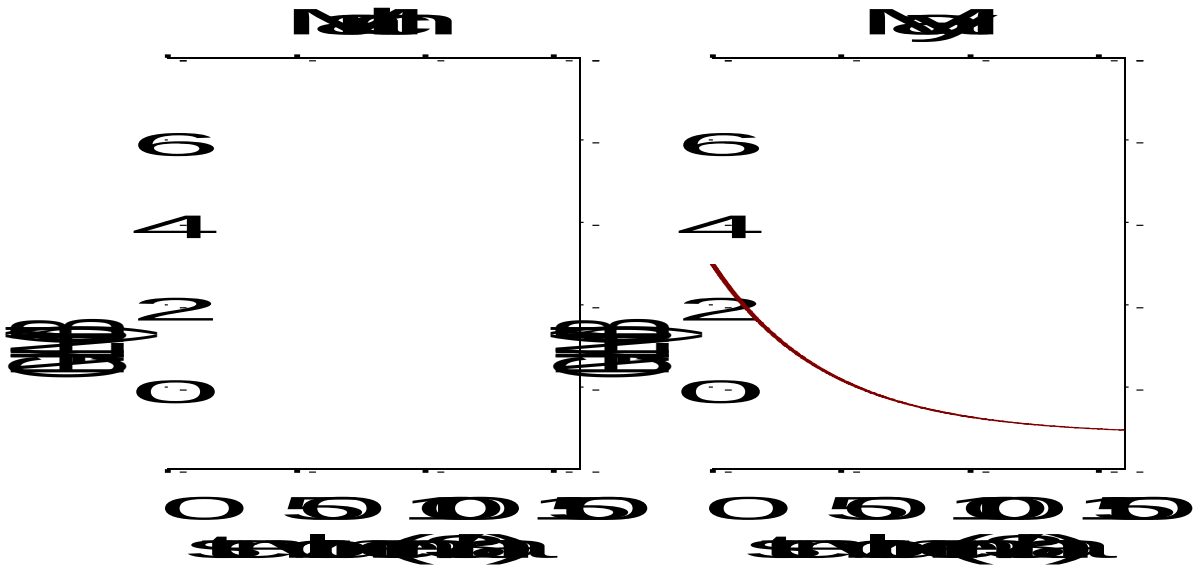

Figure 7. Scatterplots of difference between C-HV and L-HV backscatter coefficients for March and May acquisitions and stem volume, with the fitted F2P1 model for May.

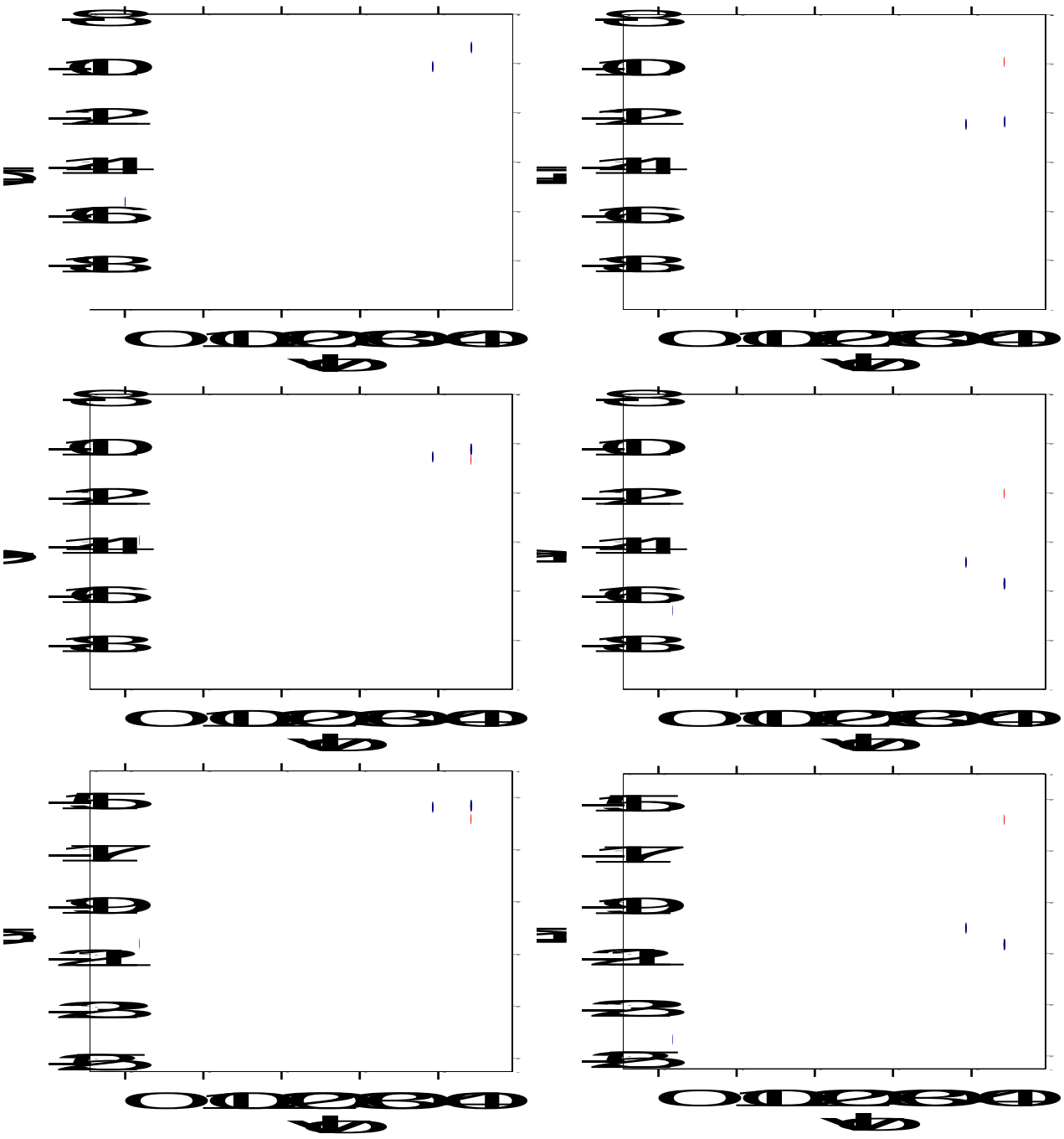

Figure 8. Scatterplots of backscatter coefficients (dB) and stem volume (*vol*, m^3/ha) for all frequencies and polarisations. The size of the data points increases with the measured snow water equivalent at the sampling point by snow fork measurements. Blue = March, red = May.

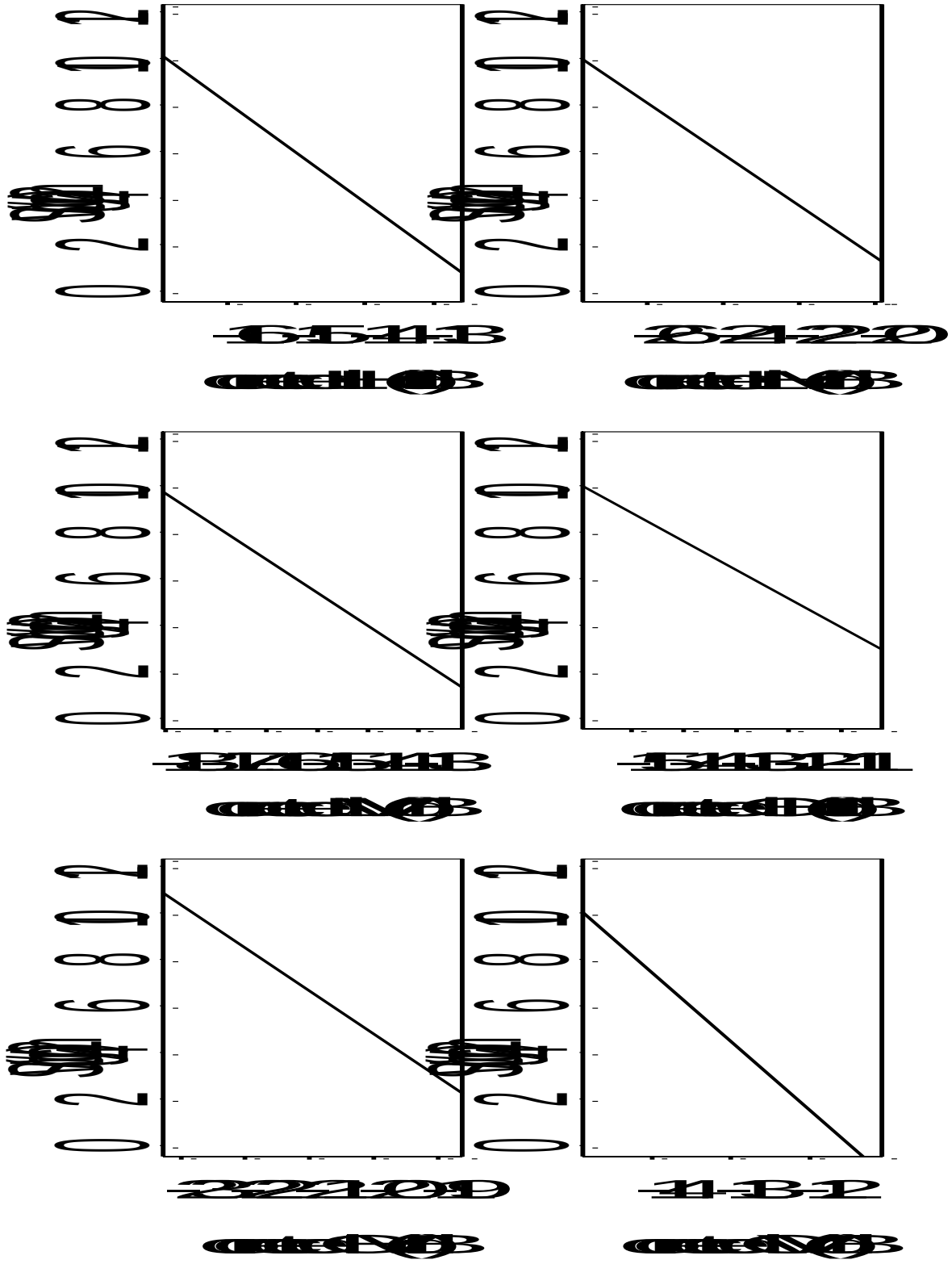

Figure 9. Scatterplots of snow water equivalent (*SW*) derived from snow fork measurements (HUT) vs. backscatter coefficients corrected for stem volume. Single regression lines.